Characterization of the endoplasmic reticulum–resident peroxidases GPx7 and GPx8 shows the higher oxidative activity of GPx7 and its linkage to oxidative protein folding

Received for publication, March 26, 2020, and in revised form, July 17, 2020 Published, Papers in Press, July 21, 2020, DOI 10.1074/jbc.RA120.013607

Shingo Kanemura[1,2,3,‡], **Elza Firdiani Sofia**[1,‡], **Naoya Hirai**[1], **Masaki Okumura**[1,3], **Hiroshi Kadokura**[1], **and Kenji Inaba**[1,*]

From the [1]*Institute of Multidisciplinary Research for Advanced Materials, Tohoku University, Katahira, Aoba-ku, Sendai, Miyagi, Japan, the* [2]*School of Science and Technology, Kwansei Gakuin University, Gakuen, Sanda, Hyogo, Japan, and the* [3]*Frontier Research Institute for Interdisciplinary Sciences, Tohoku University, Aramaki, Aza, Aoba-ku, Sendai, Miyagi, Japan*

Edited by Ruma Banerjee

Oxidative protein folding occurs primarily in the mammalian endoplasmic reticulum, enabled by a diverse network comprising more than 20 members of the protein disulfide isomerase (PDI) family and more than five PDI oxidases. Although the canonical disulfide bond formation pathway involving Ero1α and PDI has been well-studied so far, the physiological roles of the newly identified PDI oxidases, glutathione peroxidase-7 (GPx7) and -8 (GPx8), are only poorly understood. We here demonstrated that human GPx7 has much higher reactivity with H_2O_2 and hence greater PDI oxidation activity than human GPx8. The high reactivity of GPx7 is due to the presence of a catalytic tetrad at the redox-active site, which stabilizes the sulfenylated species generated upon the reaction with H_2O_2. Although it was previously postulated that GPx7 catalysis involved a highly reactive peroxidatic cysteine that can be sulfenylated by H_2O_2, we revealed that a resolving cysteine instead regulates the PDI oxidation activity of GPx7. We also determined that GPx7 formed complexes preferentially with PDI and P5 in H_2O_2-treated cells. Altogether, these results suggest that human GPx7 functions as an H_2O_2-dependent PDI oxidase in cells, whereas PDI oxidation may not be the central physiological role of human GPx8.

Most secretory and cell-surface membrane proteins undergo oxidative protein folding in the endoplasmic reticulum (ER) to acquire native conformations via disulfide bond formation and isomerization. In the mammalian ER, the reactions are catalyzed by a variety of oxidoreductases that encompass more than 20 members of the protein disulfide isomerase (PDI) family (1–5) and more than 5 PDI oxidases including ER oxidoreductin-1α (Ero1α) (6–9) and peroxiredoxin-4 (Prx4) (10–12). Some PDI family enzymes also engage in disulfide bond reduction to promote protein folding (13), the ER-associated degradation of misfolded proteins (14–16), or the ER-to-cytosol retrograde translocation of a bacterial cholera toxin and nonenveloped viruses (17–19). PDI family members typically possess thioredoxin-like domains with a *CXXC* motif at the redox-active site, thereby exerting thiol-disulfide exchange reactions with substrate proteins (1, 3). Thus, the PDI family enzymes, in combination with their upstream oxidases or reductases, constitute a diverse thiol-mediated network to maintain the proteostasis in the ER (2, 3).

Ero1α and PDI play central role in the canonical pathway of disulfide bond formation at the cost of one molecular oxygen per disulfide bond, resulting in the generation of H_2O_2 as a by-product (2, 6). Overproduction of H_2O_2 as a consequence of the Ero1α overwork causes oxidative stress in the ER, eventually leading to cell death. Therefore, the oxidative activity of Ero1α needs to be tightly controlled (20). In the mechanism of operation of mammalian Ero1α, four cysteine residues in the electron shuttle loop act also as components of a regulatory switch, which ensures strict regulation over Ero1α activity (8, 9, 20–23). An ER-resident peroxiredoxin, Prx4, metabolizes H_2O_2 and oxidizes PDI family enzymes upon return to the reduced state (24, 25). Our prior *in vitro* studies showed that ERp46 and P5, with their partner oxidase Prx4, are engaged in the rapid but promiscuous disulfide bond introduction in the initial phase of oxidative protein folding (10), whereas PDI, in concert with Ero1α, efficiently catalyzes the correction of non-native disulfide bonds and the subsequent selective formation of native disulfide bonds (26). Other oxidative pathways involving vitamin K epoxide reductase were also reported to potentially operate in the PDI reoxidation cycle (27, 28).

More recently, glutathione peroxidase-7 (GPx7) and -8 (GPx8) were identified as ER-resident PDI oxidases using H_2O_2 as a source of oxidative power (29–31). GPx family was historically named after its first identified member that catalyzes the reaction of peroxide with reduced glutathione (GSH) on its selenocysteine residue (32). Despite the absence of a GSH-binding motif and the substitution of the selenocysteine residue by Cys in GPx7 and GPx8, both the enzymes are capable of acting as peroxidases, which reduce H_2O_2 to water (29, 31, 33). GPx7-deficient cells were found to accumulate endogenous reactive oxygen species, lowering cellular viability (34, 35). Another study demonstrated that GPx7 plays a role in the alleviation of oxidative stress in breast cancer cells, esophageal cells, and adipose tissue, emphasizing the importance of GPx7 in the oxidative stress response (35–38). Both GPx7 and GPx8 were suggested to interact with Ero1α *in vivo* and possibly modulate the peroxide-generating activity of Ero1α by scavenging H_2O_2 in its proximity (29). Additionally, the Ero1α–GPx8

‡These authors contributed equally to this work.
*For correspondence: Kenji Inaba, kenji.inaba.a1@tohoku.ac.jp.

complex may serve to prevent the diffusion of H_2O_2 from the ER (39).

GPx7 and GPx8 commonly possess an essential peroxidatic cysteine residue (C_P) in the typical motif, NVAS*X*(C/U)G (Cys^{57} in GPx7 and Cys^{79} in GPx8), and a resolving cysteine residue (C_R) in the highly conserved motif of GPx family, FPCNQF (Cys^{86} in GPx7 and Cys^{108} in GPx8) (40, 41). Whereas GPx7 and GPx8 share a highly similar overall structure, their topologies are distinct in the following points: GPx7 is purely a luminal protein, whereas GPx8 has a small N-terminal cytoplasmic domain, a short transmembrane domain, and a catalytic-active domain facing the lumen (named the "luminal domain" in this work) (33). Although some structural and molecular insights have been gained into GPx7 and GPx8, the mechanistic details of GPx7/8-mediated PDI oxidation and their physiological roles in cells, especially their involvement in oxidative protein folding, still remain unclear.

In this study, we investigated the mechanistic basis of human GPx7- and GPx8-catalyzed PDI oxidation and identified their preferential substrates among PDI family members both *in vitro* and *in vivo*. We thus demonstrated that GPx7 was a much more efficient PDI oxidase than GPx8 because of even higher susceptibility of C_P to H_2O_2, in which Gln^{92} contained in the catalytic tetrad plays a critical role. Although the GPx7 catalysis was known to involve the C_P residue (31), we found that the C_R residue acts to regulate the PDI oxidation activity of GPx7. Our extensive studies also revealed that GPx7 bound PDI and P5 in H_2O_2-treated cells. Thus, human GPx7 is a potent PDI oxidase, whereas the role of human GPx8 seems largely distinct from that of GPx7 despite their structural similarity.

Results

Higher reactivity with H_2O_2 and PDI of GPx7 than that of GPx8

Although both GPx7 and GPx8 are presumed to work as PDI-dependent peroxidases (29), the reactivity of these two enzymes with H_2O_2 have not been assessed precisely. To compare their peroxidase activities, we first mixed the fully reduced form of GPx7 or the luminal domain of GPx8 (1 μM each) with different concentrations (10, 50, and 200 μM) of H_2O_2 and followed their redox state changes (Fig. 1). The aliquot samples were treated with 1 mM maleimidyl PEG-2000 (mal-PEG 2k) for quenching at the indicated time points. Although the topmost and bottom bands are identifiable as reduced and oxidized species, respectively, the intermediate band is most likely a hyperoxidized species (SO_2H or SO_3H form), in which C_R is mal-PEG modifiable, but C_P is no longer alkylated because of the hyperoxidation with H_2O_2. In support of this, the intermediate bands significantly increased at higher H_2O_2 concentrations as observed particularly with GPx8 (Fig. 1, *right panels*).

The present assay revealed much higher reactivity or affinity of GPx7 for H_2O_2 than that of GPx8; 10 μM H_2O_2 was sufficient to fully oxidize 1 μM GPx7 within 15 s after mixing, whereas most of the GPx8 remained reduced even after 5 min in the presence of 10 μM H_2O_2. Higher concentrations of H_2O_2 significantly accelerated GPx8 oxidation concomitant with increased generation of the hyperoxidized species, suggesting that the K_d for H_2O_2 value of GPx8 is much above 10 μM.

To visualize H_2O_2-driven PDI oxidation by GPx7 and the luminal domain of GPx8, reduced PDI (10 μM) was reacted with GPx7 or GPx8 (1 μM each) in the presence of 10, 50, or 200 μM of H_2O_2, and the redox-state change of PDI was monitored by mal-PEG 2k modification of free cysteines followed by nonreducing SDS-PAGE (Fig. 2*A*). Consequently, GPx7 generated significant amounts of partially and fully oxidized PDI at early time points, whereas GPx8 hardly accelerated PDI oxidation compared with H_2O_2 alone. This result is in line with the present observation that GPx7 was oxidized by H_2O_2 much more efficiently than GPx8 (Fig. 1). Of note, GPx7-mediated PDI oxidation was slower at 200 μM H_2O_2 than at 50 μM H_2O_2. This is likely explained by the greater generation of a hyperoxidized GPx7 species during the catalysis of PDI oxidation in the presence of higher concentrations of H_2O_2. In support of this notion, most of GPx7 was converted to a hyperoxidized species during the catalysis of PDI oxidation at 200 μM H_2O_2 (Fig. 2*B*). The generation of a hyperoxidized species of GPx7 was greater in the presence of reduced PDI (Fig. 2*B versus* Fig. 1, *left*, *middle*, and *bottom panel*). This observation suggests that the catalytic cycle significantly increased the hyperoxidized species via redox reactions between H_2O_2 and reduced GPx7 generated by oxidizing PDI every turnover.

A pK_a value, which determines the degree of protonation at a given pH, represents a fundamental character of protein thiol groups (42, 43). To examine whether the pK_a values of GPx7 and GPx8 can explain their different peroxidatic activities, we analyzed crystal structures of the enzymes (Protein Data Bank codes 2P31 for GPx7 and 3CYN for GPx8) using the program PROPKA3. The *in silico* analysis yielded the pK_a values of peroxidatic cysteines (C_P) of GPx7 and GPx8 to be 9.3 and 11.5, respectively. Thus, C_P in GPx8 is predicted to have exceptionally low reactivity compared with C_P in GPx7 and free cysteine in solution (pK_a of 8.3). Altogether, the results tempt us to suspect a functional role of GPx8 as a H_2O_2-scavenging peroxidase in the ER.

Essential role of a Gln residue in the catalytic tetrad of GPx7

Effective thiol-based peroxidases commonly contain a catalytic triad or tetrad including a highly reactive, C_P (40, 41). Indeed, GPx7 contains a catalytic tetrad consisting of Cys^{57}, Trp^{142}, Asn^{143}, and Gln^{92} at the active site, where Gln^{92} is predicted to stabilize thiolated or sulfenylated Cys^{57} through a hydrogen bond upon reaction with H_2O_2 (40). Although GPx8 also conserves the first three residues, Cys^{79}, Trp^{164}, and Asn^{165}, at the positions corresponding to Cys^{57}, Trp^{142}, and Asn^{143} in GPx7, respectively, we surmised that the replacement of Gln^{92} (in GPx7) to Ser^{114} (in GPx8) (Fig. 3, *A* and *B*) was a primary reason for much lower peroxidase activity of GPx8 than that of GPx7. In this context, the distance between the S_γ atom of GPx7 Cys^{57} and $O_{\epsilon 1}$ of Gln^{92} is 3.1 Å, close enough to stabilize the thiolated GPx7 C_P via a hydrogen bond to the $O_{\epsilon 1}$; meanwhile the S_γ atom of GPx8 Cys^{79} is separated from the O_γ atom of Ser^{114} by 4.8 Å, far beyond a hydrogen-bonding distance (Fig. 3*B*).

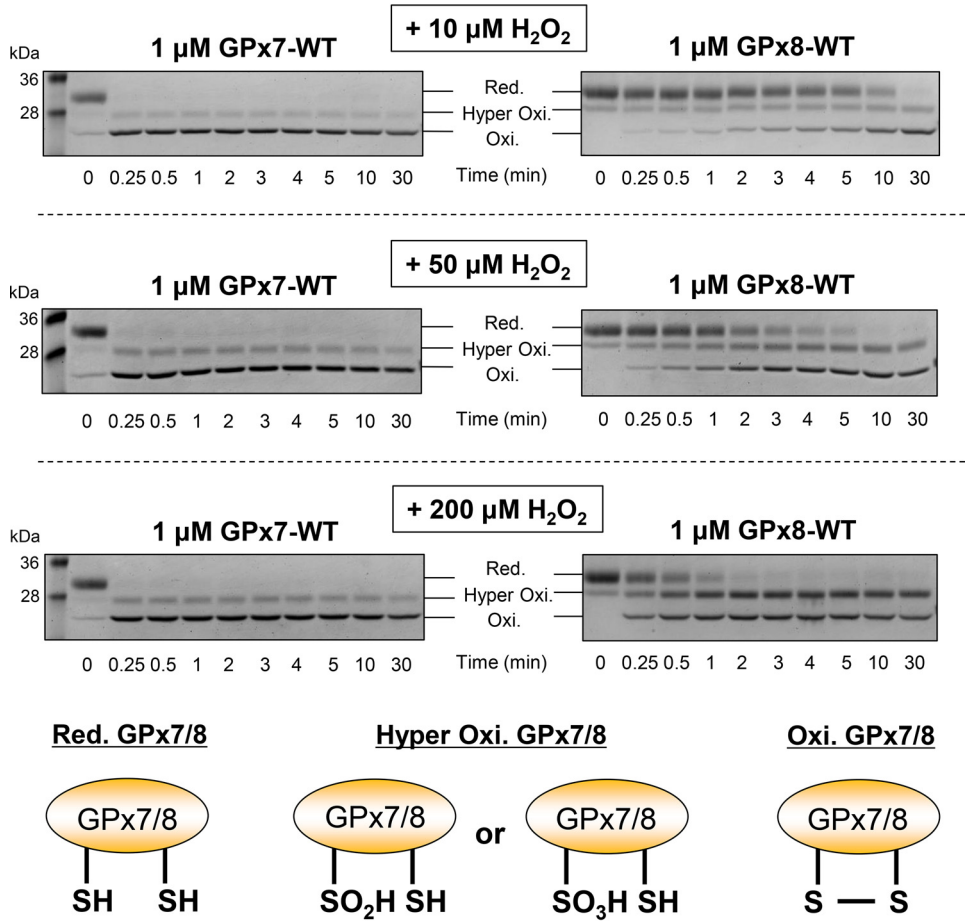

Figure 1. Reactivities of GPx7 and GPx8 with hydrogen peroxide. Time course of the redox-state change of GPx7 and the luminal domain of GPx8 during a reaction between 1 μM GPx7/8 and 10, 50, or 200 μM H_2O_2. At the indicated time points, the reaction mixture was quenched with mal-PEG 2k. GPx7 and the luminal domain of GPx8 were separated by nonreducing SDS-PAGE and stained with CBB. *Red.*, *Hyper Oxi.*, and *Oxi* denote fully reduced, hyperoxidized, and fully oxidized species of GPx7/8, respectively. A graphic representation of the redox states of GPx7/8 is shown *below* the gel images. A representative gel image of three experiments at each condition is displayed.

To explore the importance of the C_P-neighboring residues in the different peroxidatic activities of GPx7 and GPx8, we constructed swap mutants where Gln is mutated to Ser in GPx7 (GPx7 Q92S) and vice versa in the luminal domain of GPx8 (GPx8 S114Q). In the result, the GPx7 swap mutation greatly compromised the GPx7 reactivity with H_2O_2 (Fig. 3*C*, *left panels*), leading to the abolishment of PDI oxidation activity (Fig. 3*D*, *left panel*). Notably, GPx7 Q92S exhibited a similar rate in H_2O_2-dependent oxidation as GPx8, although the latter generated larger amount of hyperoxidized species than the former at both 10 and 50 μM H_2O_2 (Figs. 1 and 3*C*, *left panel*). It is also noteworthy that GPx8 S114Q greatly increased the GPx8 reactivity with H_2O_2, leading to more efficient PDI oxidation in the presence of 10 μM H_2O_2 (Fig. 3, *C* and *D*, *upper right panel*). However, GPx8 S114Q only partially oxidized PDI at 50 μM H_2O_2 (Fig. 3*D*, *lower right panel*), likely because of the predominant formation of the hyperoxidized form as observed for GPx7 WT in the presence of 200 μM H_2O_2 and 10 μM reduced PDI (Fig. 2*B*, *right panel*). Even without reduced PDI, GPx8 S114Q indeed generated a considerable amount of hyperoxidized species upon reaction with 50 μM H_2O_2 (Fig. 3*C*, *lower right panel*). Collectively, we conclude that Gln^{92} acts as an essential residue for high reactivity of GPx7 with H_2O_2 and hence effective oxidation of PDI by the enzyme.

GPx7 Cys^{86} plays a critical role in the regulated oxidative activity of GPx7

Three-dimensional structures of reduced forms of GPx7 and GPx8 have high similarity, in which the locations and orientations of C_P and C_R in GPx7 are almost identical to those in GPx8 (29). The S_γ atoms of C_P and C_R are separated by ~11 Å in both the enzymes, suggesting that a large conformational change is required for formation of an intramolecular disulfide bond between these two cysteines (30). Given the situations, two alternative mechanisms have been proposed for GPx7/GPx8-mediated PDI oxidation: a one-cysteine mechanism in which the C_P acts as the sole redox center that reacts with both H_2O_2 and PDI and a two-cysteine mechanism in which an intramolecular disulfide bond between C_P and C_R is formed preceding the oxidation of PDI (30, 33).

To investigate which of the mechanisms is primarily exerted by GPx7 and GPx8, we constructed single-Cys mutants of the enzymes in which C_R was mutated to alanine: C86A for GPx7 and C108A for GPx8. Of interest, the results demonstrated that GPx7 C86A oxidized PDI more efficiently than GPx7 WT (Figs. 2*A*, *left middle panel*, and 4*A*, *left panel*), suggesting that a one-cysteine mechanism is more competent in PDI oxidation than a two-cysteine mechanism and that GPx7 WT exerts primarily a

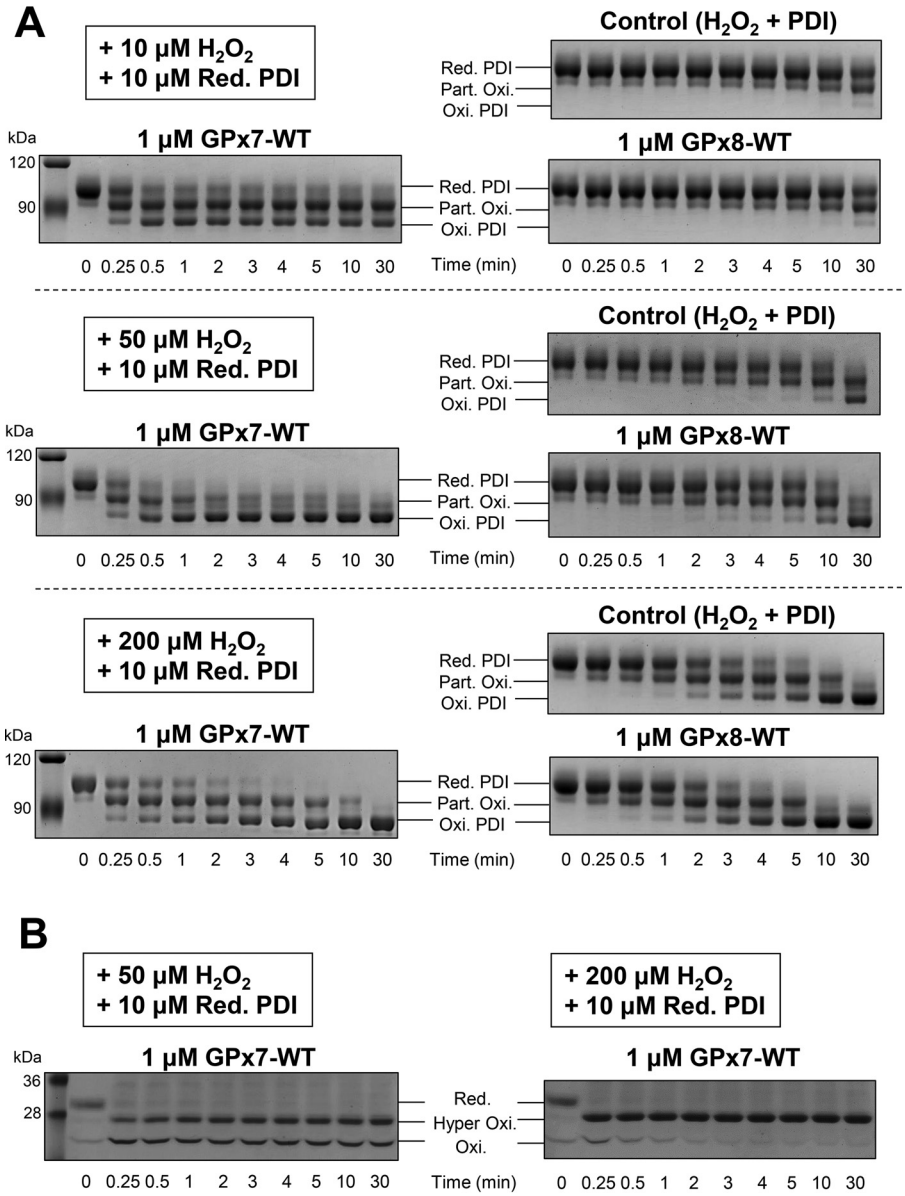

Figure 2. GPx7/GPx8-catalyzed oxidation of PDI in the presence of hydrogen peroxide. *A*, time course of the redox-state changes of PDI during noncatalyzed, GPx7-catalyzed, and GPx8-catalyzed PDI oxidation. All experiments were initiated by mixing 10, 50, and 200 μM H_2O_2 into the mixture of reduced PDI (10 μM) and GPx7 or the luminal domain of GPx8 (1 μM) in buffer containing 50 mM Tris/HCl (pH 7.4) and 300 mM NaCl. At the indicated time points, the reaction mixture was alkylated with mal-PEG 2k. The redox states of PDI were separated by nonreducing SDS-PAGE and stained with CBB. *Red. PDI*, *Part. Oxi.*, and *Oxi. PDI* denote fully reduced, partially oxidized, and fully oxidized species of PDI, respectively. *B*, time course of the redox-state change of GPx7 WT (1 μM) during the catalysis of oxidation of PDI (10 μM) in the presence of 50 or 200 μM H_2O_2. A representative gel image of three experiments at each condition is displayed in both *A* and *B*.

two-cysteine mechanism or both one- and two-cysteine. By contrast, GPx8 C108A oxidized PDI even less efficiently than GPx8 WT (Figs. 2*A*, *middle right panel*, and 4*A*, *right panel*), indicating the necessity of C_R for the GPx8-mediated PDI oxidation. Thus, GPx8 is likely to utilize a two-cysteine mechanism exclusively.

For GPx7 to exert a one-cysteine mechanism with high efficiency, its C_P must be very reactive with H_2O_2. To verify that it is indeed the case, we investigated the susceptibility of GPx7 C86A to H_2O_2-mediated hyperoxidation. As expected, GPx7 C86A was rapidly hyperoxidized with 50 μM H_2O_2, whereas its counterpart, GPx8 C108A, was much less sensitive to H_2O_2 (Fig. 4*B*). To further compare the oxidative activities of GPx7 WT and C86A, we investigated oxidative folding of RNase A catalyzed by these two using gel-shift assay (Fig. 4*C*). The results demonstrated that GPx7 C86A oxidized RNase A much more rapidly than GPx7 WT. Accordingly, GPx7 C86A restored RNase A activity more quickly than GPx7 WT (Fig. 4*D*). Thus, GPx7 can be a more competent H_2O_2-dependent oxidase by exerting a one-cysteine mechanism exclusively on the highly reactive peroxidatic cysteine.

To explore whether GPx7 WT primarily employs a one- or two-cysteine mechanism, we examined the PDI concentration dependence of the rate of PDI oxidation by GPx7 WT and C86A by performing the NADPH consumption assay. We predicted that, at higher PDI concentrations, a one-cysteine

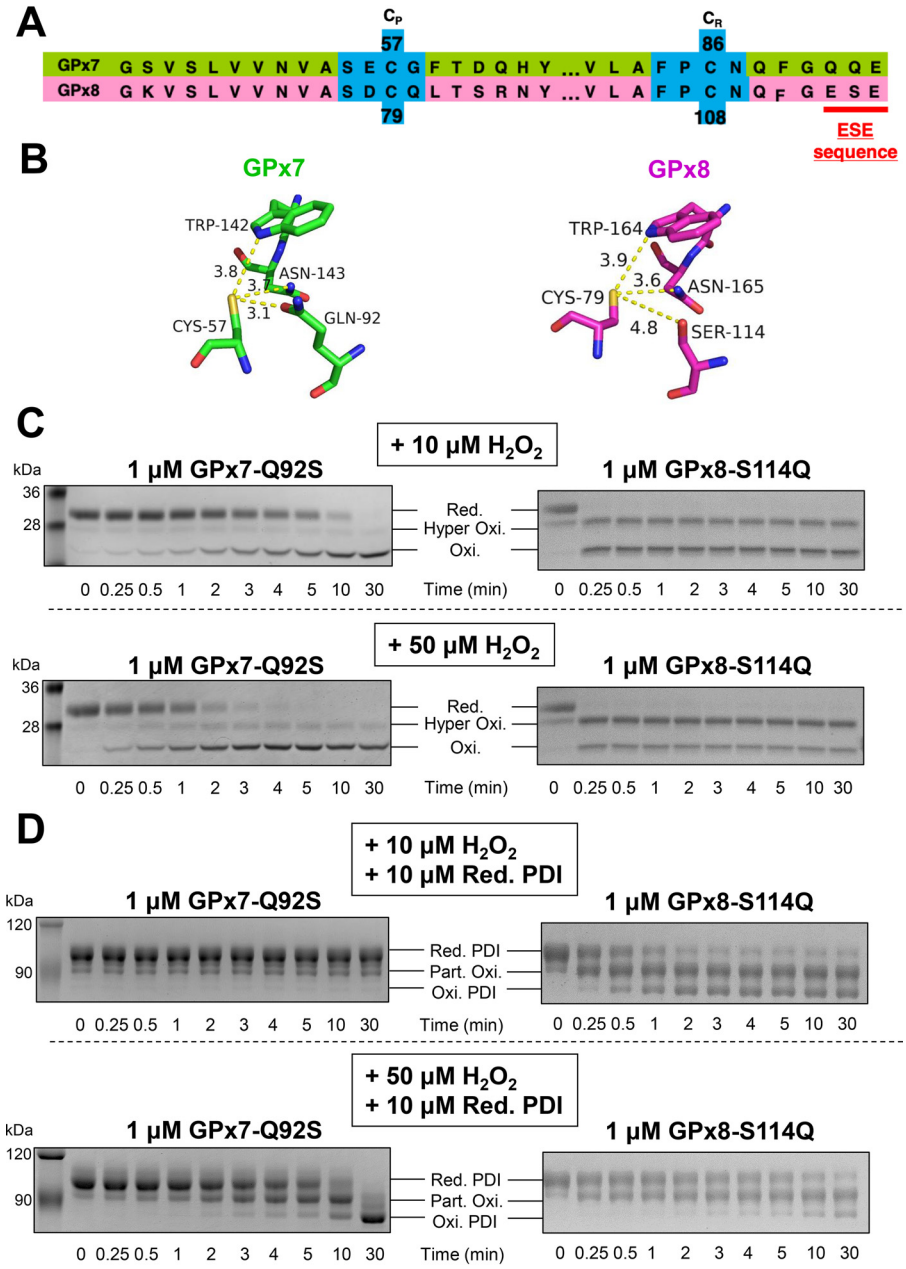

Figure 3. Effects of a mutation at the catalytic tetrad on the reactivity of GPx7/8 with hydrogen peroxide and PDI. *A*, amino acid sequence alignment in the C_P- and C_R-neighboring regions of human GPx7 and GPx8. *B*, catalytic tetrads of GPx7 and GPx8 involving a peroxidatic cysteine and its neighboring Trp and Gln/Ser residues. In GPx7, the $O_{\epsilon 1}$ atom of the Gln^{92} side chain is distant from the S_γ atom of Cys^{57} by 3.1 Å, whereas the O_γ atom of Ser^{114} in GPx8 side chain is separated from the S_γ atom of Cys^{79} by 4.8 Å. *C*, time course of the redox-state changes of GPx7 and GPx8 swap mutants (GPx7 Q92S and GPx8 S114Q) during a reaction between 1 μM GPx7/8 and 10 or 50 μM H_2O_2. At the indicated time points, the reaction mixture was alkylated with mal-PEG 2k. *D*, time course of the redox-state change of PDI during a reaction between 1 μM GPx7 swap mutant (GPx7 Q92S) or GPx8 swap mutant (GPx8 S114Q) and 10 μM PDI in the presence of 10 or 50 μM H_2O_2. A representative gel image of three experiments at each condition is displayed in *C* and *D*.

mechanism gets more predominant over a two-cysteine mechanism because, under such conditions, reduced PDI should more likely win the race of nucleophilic attack to a sulfenylated C_P against the C_R residue of the same GPx7 molecule (Fig. 5*A*). Given that, the oxidative activity of GPx7 WT will approach that of GPx7 C86A as the concentration of PDI increases. However, higher PDI concentrations did not render the initial NADPH consumption rates of GPx7 WT and C86A closer to each other (Fig. 5, *B* and *C*). It is thus conceivable that, regardless of the PDI concentration, GPx7 WT primarily employs a two-cysteine mechanism, resulting in the slower oxidation of PDI and hence the slower oxidative folding of a downstream substrate than GPx7 C86A (Fig. 4).

Preferential oxidation substrate of GPx7 among PDI family members

Previous studies by us and others suggest that PDI oxidases have high selectivity against the PDI family members in the disulfide bond formation network (10, 12, 21, 29, 44, 45). The

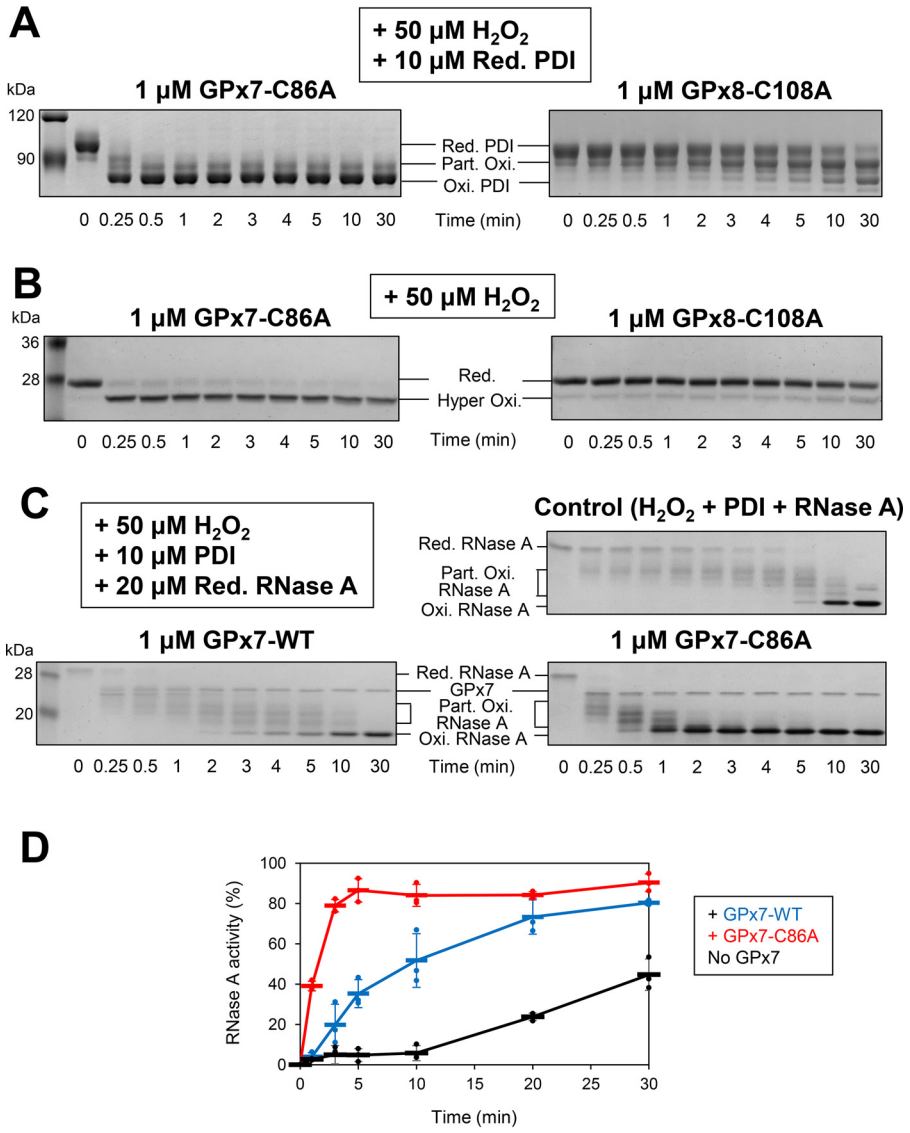

Figure 4. Effects of a C_R-residue mutation on the oxidative activities of GPx7/8. *A*, time course of the redox-state change of PDI during a reaction between 1 μM GPx7 C86A or GPx8 C108A and 10 μM reduced PDI in the presence of 50 μM H_2O_2. At the indicated time points, the reaction mixture was alkylated with mal-PEG 2k. *B*, time course of the redox-state change of GPx7 C86A and GPx8 C108A after mixture with 50 μM H_2O_2. At the indicated time points, the reaction mixture was alkylated with mal-PEG 2k. *Red.* and *Hyper Oxi.* denote fully reduced and hyperoxidized species of the GPx7/8 mutants, respectively. *C*, time course of the redox state changes of reduced/denatured RNase A (20 μM) during oxidation by 10 μM PDI and 1 μM GPx7 WT or C86A in the presence of 50 μM H_2O_2. At the indicated time points, the reaction mixture was alkylated with AMS. *Red. RNase A*, *Part. Oxi. RNase A*, and *Oxi. RNase A* denote fully reduced, partially oxidized, and fully oxidized species of RNase A, respectively. A representative gel image of three experiments at each condition is displayed in *A*, *B*, and *C*. *D*, recovery of RNase A activity during oxidative folding catalyzed by 10 μM PDI and 1 μM GPx7 WT or C86A in the presence of 50 μM H_2O_2 ($n = 3$, means ± S.D.).

present study indicated that whereas the PDI oxidation activity of GPx8 is minimal, GPx7 has significant PDI oxidation activity. To investigate GPx7 preference for the PDI family members, five representative members of the PDI family (PDI, ERp46, P5, ERp57, and ERp72), either independently or in a mixture of five, were subjected to oxidation by GPx7 in the presence of H_2O_2, and the time-dependent changes of their redox states were monitored by immunoblotting with an antibody against each PDI (Fig. 6*A*). The results of GPx7-catalyzed single-PDI oxidation demonstrated that the enzyme was a versatile oxidase to all PDI family members tested (Fig. 6, *A* and *B*, *left panels*). By contrast, when GPx7 was reacted with the mixture of PDIs, ERp46 and ERp72 were oxidized in greatest amount compared with the other three PDIs (Fig. 6, *A* and *B*, *right panels*), suggesting that GPx7 has significant preference for these two members. Interestingly, even though P5 seemed a good substrate of GPx7 in the single-PDI oxidation assay, P5 remained fully reduced in the mixture of PDIs, probably because of the competitive inhibition by the other PDI family members. Unlike P5, ERp46 and ERp72 were significantly oxidized by GPx7 even in presence of the other representative PDIs (Fig. 6, *A* and *B*, *right panels*).

H_2O_2-induced complex formation between PDIs and GPx7/8 in cells

To gain insights into physiological redox partners of GPx7 and GPx8, we next transfected HeLa cells with plasmids

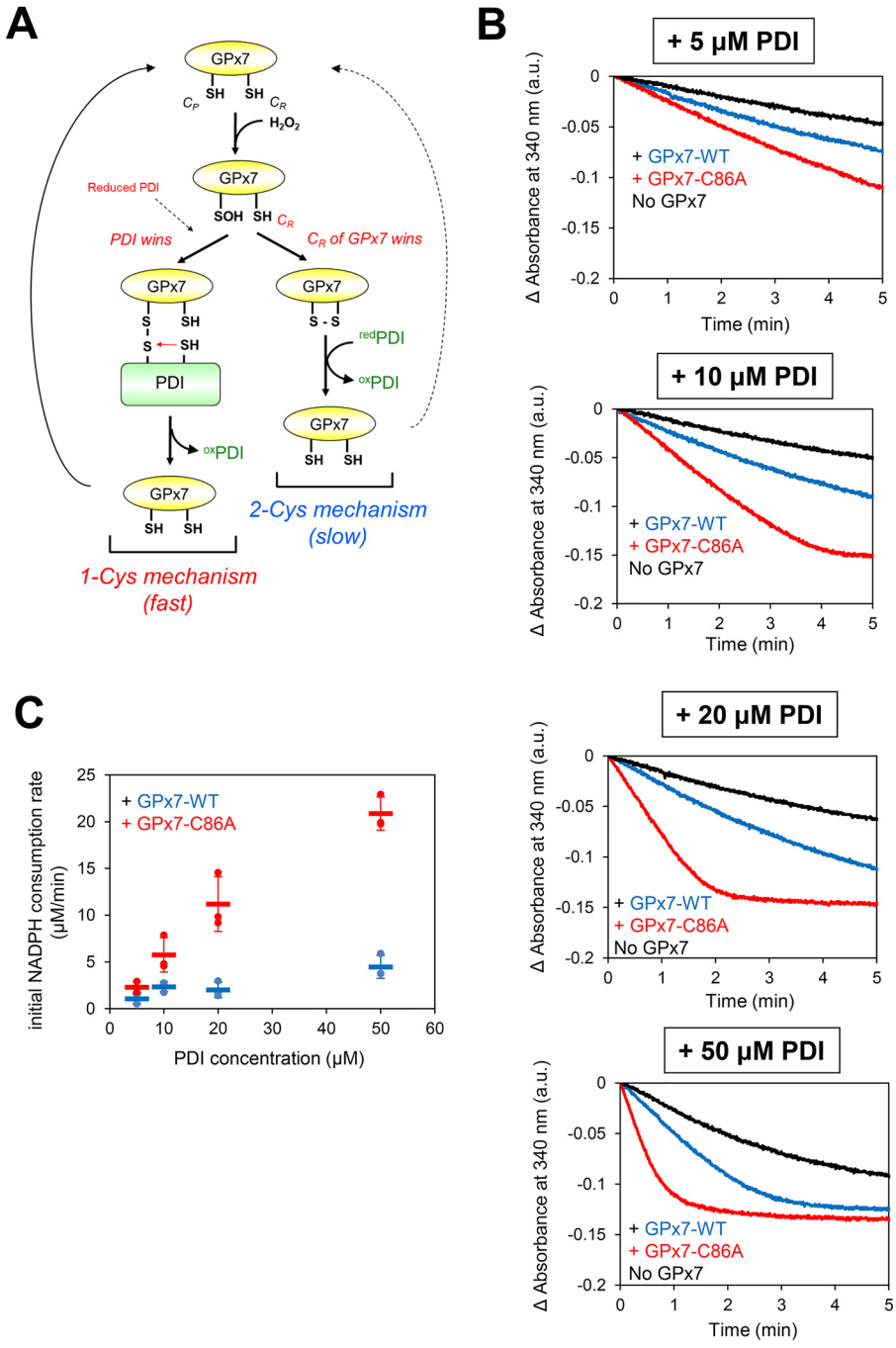

Figure 5. Effects of PDI concentration on the oxidative activities of GPx7 WT and C86A. *A*, alternative (one- or two-cysteine) mechanism of GPx7 in the catalysis of PDI oxidation. A peroxidatic cysteine (C_P) of GPx7 is readily sulfenylated upon reaction with H_2O_2, followed by the race between reduced PDI and a resolving cysteine (C_R) of the same GPx7 molecule against the sulfenylated C_P. *B*, NADPH consumption coupled to PDI oxidation catalyzed by GPx7 WT or GPx7 C86A was monitored by measuring absorbance change at 340 nm. All experiments were initiated at 30 °C by mixing 50 μM H_2O_2 into the mixture of reduced PDI (5–50 μM), GSH (1 mM), GR (1 unit), NADPH (200 μM), and GPx7 WT or GPx7 C86A (1 μM) in buffer containing 50 mM Tris/HCl (pH 7.4) and 300 mM NaCl. Representative data of three experiments at each condition are displayed. *C*, plots of the initial NADPH consumption rate (mM/min) during the catalysis of GPx7 WT or GPx7 C86A as a function of PDI concentrations. Note that the rates were calculated by subtracting the rate of noncatalyzed reaction (No GPx7) from those of GPx7-catalyzed reactions (GPx7 WT or C86A) ($n = 3$, means = ±S.D.).

expressing FLAG-tagged Prx4, GPx7, or full-length GPx8; treated the cells with or without 0.5 mM H_2O_2 for 10 min; and alkylated the free cysteines with *N*-maleimide (NEM) as described under "Experimental procedures," followed by immunoprecipitation and immunoblotting with an antibody against each PDI family member (Fig. 7). We thus reproduced our previous observation that Prx4 most preferentially bound ERp46 and P5 in an H_2O_2-independent manner in cells (10). Notably, GPx7 bound PDI only slightly and did not bind the other PDI family members without H_2O_2 (Fig. 7). However, H_2O_2 treatment significantly increased amounts of PDI and P5 bound to GPx7. A similar observation was made with GPx8 despite even smaller amounts of PDI and P5 co-immunoprecipitated with GPx8 (Fig. 7). Thus, GPx7 displayed PDI preference different from Prx4,

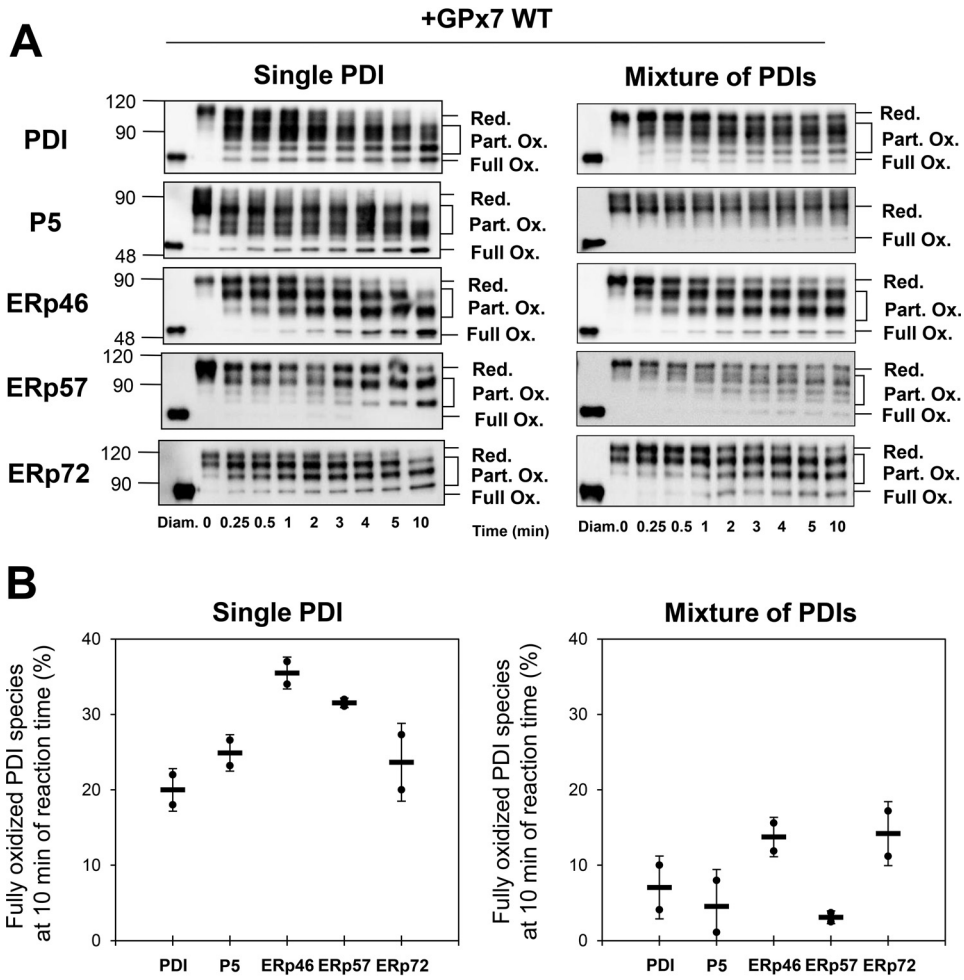

Figure 6. Preferential oxidation of PDI family members by GPx7. *A*, time course of redox state changes of PDI family members (PDI, P5, ERp46, ERp57, and ERp72) during the catalysis of PDI oxidation by GPx7 WT. The reactions were initiated by reacting 5 μM reduced PDIs (single or a subset of five) with 0.5 μM GPx7 WT in the presence of 50 μM H_2O_2. The reactions were quenched by cysteine alkylation with mal-PEG 2k at the indicated time points, followed by gel separation using nonreducing SDS-PAGE and monitored by immunoblotting with antibodies to each PDI family member. A representative gel image of two experiments at each condition is displayed. *Red.*, *Part. Ox.*, and *Full Ox. PDI* denote fully reduced, partially oxidized, and fully oxidized, respectively. *B*, quantification of the percentage of fully oxidized PDIs species generated after 10 min of reaction ($n = 2$, means ± S.D.).

although both the peroxidases bound their preferential PDIs more tightly in the presence of H_2O_2. Notably, the intracellular redox partners of GPx7 did not coincide with its preferential substrates identified by *in vitro* experiments (Fig. 6), suggesting the presence of mediator proteins that link GPx7 to its physiological redox partners (see also "Discussion").

Discussion

Previously, GPx7 and GPx8 were demonstrated to be capable of utilizing Ero1α-derived H_2O_2 in cells (29). Although GPx8 was reported to interact directly with Ero1α and scavenge the neighboring H_2O_2 molecule (39), the present work revealed that GPx7 had much higher reactivity with H_2O_2 than GPx8, leading to the more efficient PDI oxidation. Although the affinity for H_2O_2 of GPx7 was not precisely determined in this study, 10 μM H_2O_2 was sufficient to oxidize GPx7 rapidly (Fig. 1). It is thus conceivable that GPx7 could compete with Prx4, another ER-resident peroxidase with a micromolar range of affinity for H_2O_2, for reacting with H_2O_2 if these two enzymes co-localize in the same compartment of the ER. However, considering that unlike GPx7, Prx4 does not scavenge Ero1α-generated H_2O_2 efficiently in cells (39), these two enzymes seem likely to have distinct physiological roles in the ER.

Reactivity of a given cysteine residue depends on the propensity of its thiolate form, which is quantitatively expressed as pK_a (46). However, pK_a is not the sole factor that determines the reactivity of a peroxidatically active cysteine with H_2O_2 (43, 47). The active sites of GPx7 and GPx8 consist of a catalytic tetrad including Cys, Trp, Asn, and Gln/Ser residues. We here demonstrated that the Gln^{92} residue in the catalytic tetrad of GPx7 is essential for the enhanced reactivity of GPx7 C_P with H_2O_2, probably because Gln^{92} serves to stabilize the sulfenylated C_P species via hydrogen bonding (Figs. 3 and 4*B*). Gln^{92} is highly conserved among all GPx family members but GPx8, in which Gln is substituted by Ser^{114}. In this regard, Ser^{114} can be interpreted to have an inhibitory role in the H_2O_2-scavenging activity of GPx8 (39), possibly providing GPx8 with other physiological functions in cells.

The present study also demonstrates that GPx7 WT preferentially employs a two-cysteine mechanism in oxidizing PDI, whereas the GPx7 C86A mutant oxidizes PDI at a much higher

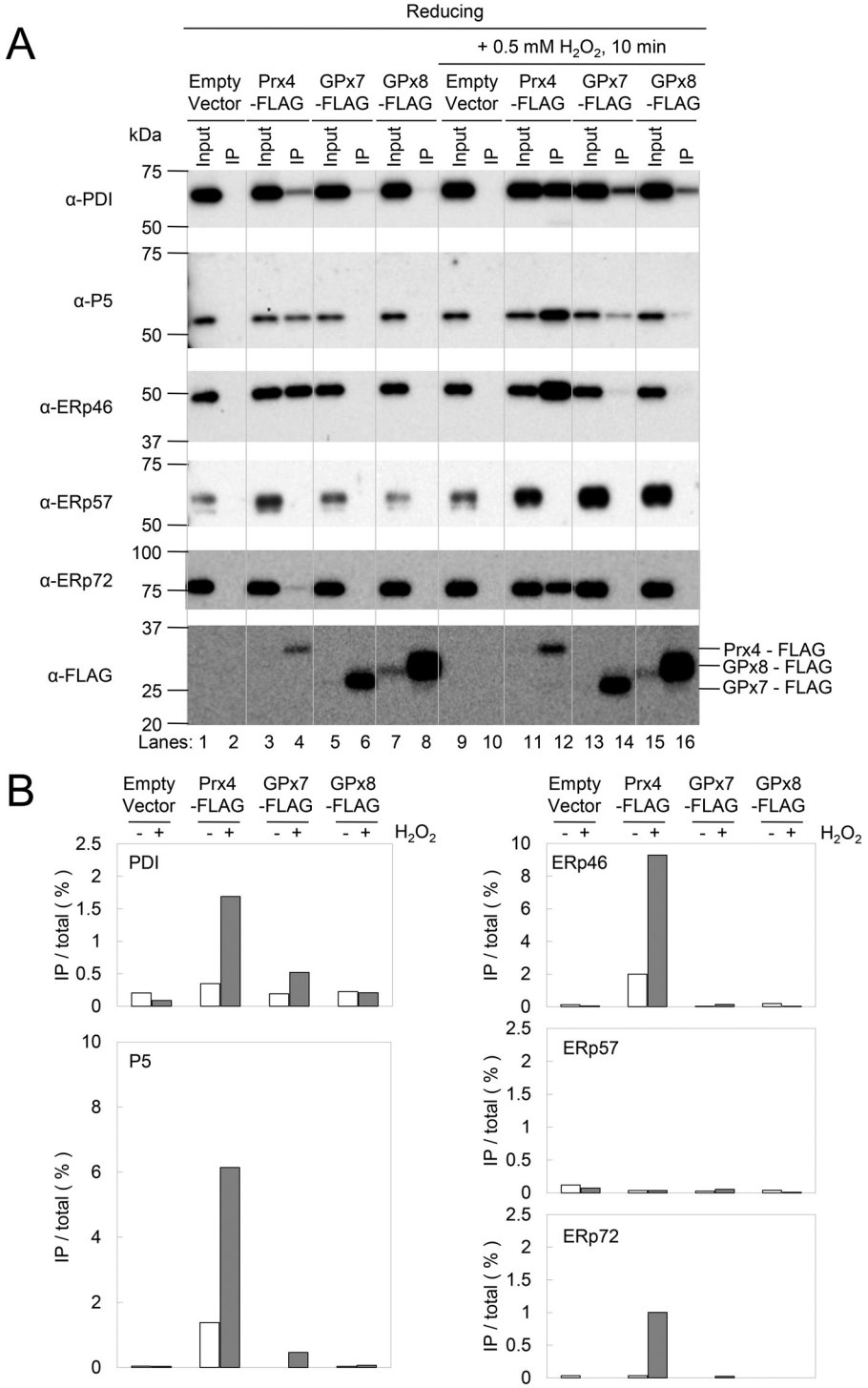

Figure 7. Complex formations of Prx4, GPx7 and GPx8 with PDI family members in cells. *A*, HeLa cells were transfected with pcDNA3.1$^+$ (empty vector) (*lanes 1*, *2*, *9*, and *10*), pCMV-Gg PRX4 (encoding PRX4-FLAG) (10) (*lanes 3*, *4*, *11*, and *12*), pES104 (encoding GPx7-FLAG) (*lanes 5*, *6*, *13*, and *14*), or pES105 (encoding full-length GPx8-FLAG) (*lanes 7*, *8*, *15*, and *16*), grown in Dulbecco's modified Eagle's medium supplemented with 10% fetal bovine serum for 24 h, treated with 0.5 mM H_2O_2 (*lanes 9–16*) for 10 min or not (*lanes 1–8*), washed twice with PBS, treated with 10% TCA, and subjected to alkylation with NEM (51). The NEM-treated cell lysates were subjected to immunoprecipitation with anti-FLAG M2 magnetic beads (Sigma) to purify complexes containing FLAG-tagged proteins. The immunoprecipitates were separated by reducing SDS-PAGE, and PDI family members and FLAG-tagged constructs contained in the immunoprecipitates were detected with antibodies to the indicated PDI family members or horseradish peroxidase-conjugated antibody to FLAG. *Lanes 1*, *3*, *5*, *7*, *9*, *11*, *13*, and *15* contained 1 μg of NEM-treated cell lysate (*Input*). *Lanes 2*, *4*, *6*, *8*, *10*, *12*, *14*, and *16* contained immunoprecipitates (*IP*) obtained from 50 μg of NEM-treated cell lysate. The positions of the FLAG-tagged constructs were indicated on the *right* in the *bottom panel*. *B*, the band intensities of PDI family members in the input and immunoprecipitate lanes on *A* were quantified using ImageJ 1.50i. PDI family members immunoprecipitated with each FLAG-tagged peroxidase are shown as a percentage of total PDIs in the cell lysate. The experiments were performed once.

rate via a one-cysteine mechanism. GPx7 C_P (Cys57) is oxidized by H_2O_2 to generate sulfenylated C_P, which can in turn react with either reduced PDI or the C_R residue of GPx7 itself. The predominant usage of a two-cysteine mechanism by GPx7 suggests faster nucleophilic attack by the C_R residue of the same molecule than by the active-site cysteines of PDI (Fig. 6*A*). Obviously, two-cysteine mechanism drives a much slower catalytic cycle than one-cysteine. This observation suggests that the intermolecular disulfide transfer from a Cys^{57}–Cys^{86} pair of GPx7 to the PDI active sites is a rate-limiting step of the GPx7-mediated PDI oxidation cycle. In other words, the presence of a C_R residue serves to regulate the oxidative activity of GPx7. In this context, the selection of one- or two-cysteine mechanism by GPx7 could be an effective strategy to maintain the redox homeostasis in the ER, as is the similar case with Ero1α, which tightly modulates its oxidative activity through the disulfide bond rearrangement among the four regulatory cysteines in response to the redox environment in the ER (7–9, 23). However, the higher concentrations of reduced PDI did not greatly enhance the oxidative activity of GPx7 WT (Fig. 5), making it unlikely that the switching from a two-cysteine to one-cysteine mechanism is induced in GPx7 when the ER environment becomes more reducing. Another possible physiological meaning of the two-cysteine mechanism is to prevent overoxidation of the peroxidatic Cys in GPx7, thereby keeping the enzyme active. Collectively, the two-cysteine mechanism of GPx7 is likely to play significant roles in maintaining the ER in the moderately oxidizing environment.

In the previous study, Ero1α was shown to preferentially oxidize PDI, and to a lesser extent ERp46, whereas Prx4 preferential oxidation substrates were P5 and ERp46 (10, 12, 44). Here we demonstrated that whereas GPx7 preferentially oxidized ERp46 and ERp72 *in vitro*, the enzyme bound PDI and P5 in H_2O_2-treated cells. The complex formation between GPx7 and P5 in cells suggests that some third-party proteins may mediate the interaction between these two. In agreement with this notion, GPx7 was reported to form a disulfide-linked complex with BiP, an ER-resident chaperone under oxidative stress conditions (35), whereas P5 targets BiP client proteins (48). Moreover, the preceding work reported that large ER-localized multiprotein complexes including various molecular chaperones such as BiP, GRp94, PDI, ERdj3, Hsp40, cyclophilin B, ERp72, GRP170, UDP-glucosyltransferase, and SDF2-L1 are formed in the ER (49). GPx7 may be one of the as-yet-unidentified components contained in this multiprotein complex, although further extensive studies are required to clarify the diverse interaction network involving GPx7 in cells.

In conclusion, the present work demonstrates that whereas GPx7 is an efficient PDI peroxidase, its phylogenic cousin GPx8 does not possess an efficient catalytic activity. GPx7 and GPx8 are similar in overall structure, such that they could share the same H_2O_2-scavenging mechanism involving their catalytic cysteine pairs. However, the different local environments near the cysteines give rise to the strikingly different reactivity with H_2O_2 of these two peroxidases. Although these two enzymes appear to fulfill distinct physiological roles in cells, it will be interesting to see whether GPx8 can function as a backup enzyme of GPx7 under some special situations such as a highly reducing redox environment or a highly H_2O_2 abundant condition in the ER.

Experimental procedures

Plasmids

Plasmids for overexpression of GPx7 and the luminal domain of GPx8 in *Escherichia coli* (pKEHS780 and pVD54, respectively) (29) were kind gifts from Dr. Lloyd Ruddock (University of Oulu). GPx7 and GPx8 Cys–Ala mutants were constructed by using the QuikChange site-directed mutagenesis kit (Agilent Technologies).

Primers and templates used to construct following plasmids are listed in Table 1. Plasmid pES101 (encoding GPx7) was constructed by assembling three DNA fragments using the Gibson assembly kit (New England Biolabs). The DNA fragments used were a fragment amplified from pcDNA3.1$^+$ (Invitrogen) with primers NeoRH1 and gpx7E1, a fragment amplified from pKEHS780 with primers gpx7E2 and gpx7E4, and a fragment amplified from pcDNA3.1$^+$ with primers NeoRH2 and gpx7E3. Plasmid pES102 that expresses the luminal domain of GPx8 in the ER and plasmid pES103 (encoding GPx8) were constructed by assembling fragments amplified using a template and a primer set indicated on Table 2. Plasmids pES104 (encoding GPx7-FLAG on pcDNA3.1$^+$) and pES105 (encoding GPx8-FLAG on pcDNA3.1$^+$) were constructed by inserting a triple FLAG sequence in front of the KDEL sequence of these proteins. They were constructed also by assembling fragments amplified using a template and a primer set indicated on Table 2.

Protein overexpression and purification

Plasmids for overexpression of GPx7, the luminal domain of GPx8, PDIs, and their mutants were transformed into *E. coli* BL21(DE3). Cells harboring the plasmids were grown at 30 °C and induced by the addition of 0.5 mM isopropyl β-D-thiogalactopyranoside at an A_{600} of 0.5. The cells were cultured for an additional 4 h at 30 °C and then harvested. To purify GPx7, GPx8, and their mutants, cells in buffer A (50 mM Tris/HCl, pH 8.1, 0.3 M NaCl, and 1 mM phenylmethylsulfonyl fluoride) were disrupted using a microfluidizer (Niro Soavi PA2K). After centrifugation of the cell lysate to remove cellular components at 12,000 rpm for 20 min, the supernatant was loaded onto an open nickel–nitrilotriacetic acid–Sepharose column (Qiagen). The column was washed with buffer A containing 20 mM imidazole, and the proteins were eluted with buffer A containing 200 mM imidazole. The eluted sample was concentrated to 500 μl by filtration using Amicon Ultra filter units (molecular weight cutoff, 10,000; Millipore), applied to a Superdex 75 size-exclusion column (GE Healthcare) pre-equilibrated with 50 mM Tris/HCl (pH 8.1), 0.3 M NaCl, and 1 mM EDTA and finally eluted with the same buffer.

To purify PDIs, the supernatant of the cell lysate was applied to the open nickel–nitrilotriacetic acid–Sepharose column. Fractions eluted with 200 mM imidazole were further purified

Table 1
Primer sequences

Name	Sequence (5′ → 3′)
gpx7E1	GAGCAGCCACGCCGCTGCCACCGTCGCCGCCACCATGGTGGCGGTACCAAGCTTAAGTTTAAACGGCTAG
gpx7E2	GTGGCAGCGGCGTGGCTGCTCCTGTGGGCTGCGGCCTGCGCGCAGCAGGAGCAGGACTTCTAC
gpx7E3	TCTAGAGGGCCCGTTTAAACC
gpx7E4	GGTTTAAACGGGCCCTCTAGATTATAAGTCTTCTCGCTTCAGTAGG
gpx7E5	CCATGACGGAGATTATAAAGATCATGACATCGACTACAAGGATGACGATGACAAGTCCGGAAAGCGAGAAGACTTATAATCTAGAGG
gpx7E6	GATCTTTATAATCTCCGTCATGGTCTTTGTAGTCTCCGGACTTCAGTAGGATGAGCTTCCTCAC
gpx8E1	GATTTTAGGTTTGAGGAATTTCATGGTGGCGGTACCAAGCTTAAGTTTAAACGC
gpx8E2	ATGAAATTCCTCAAACCTAAAATC
gpx8E4	GGTTTAAACGGGCCCTCTAGATCATAGATCCTCTTTCTTTTTTATGATCAC
gpx8fE5	CAAAACTGCAAATACCTTTGCTCTGGGCCCGGAACATTTTAGCGGGTAAGCTGCAAGAGGCTCCATGGTGGCGGTACCAAGC
gpx8fE6	GCAAAGGTATTTGCAGTTTTGCTGTCTATAGTTCTATGCACAGTAACGCTATTTCTTCTACAACTAAAATTCCTCAAACCTAAAATCAA-CAGC
gpx8E9	GACCATGACGGAGATTATAAAGATCATGACATCGACTACAAGGATGACGATGACAAGTCCGGAAAAGAGGATCTATGATCTAGAGGG
gpx8E10	GATCTTTATAATCTCCGTCATGGTCTTTGTAGTCTCCGGACTTCTTTTTTATGATCACTTGTCTAACCAG
NeoRH1	CTGAGCGGGACTCTGGGGTTCG
NeoRH2	ATTTCGAACCCCAGAGTCCCGC

Table 2
Template and primers used to construct pES plasmids

	Fragment 1		Fragment 2		Fragment 3	
Plasmids	Template	Primers	Template	Primers	Template	Primers
pES101	pcDNA3.1$^+$	NeoRH1 + gpx7E1	pKEHS780	gpx7E2 + gpx7E4	pcDNA3.1$^+$	NeoRH2 + gpx7E3
pES102	pcDNA3.1$^+$	NeoRH1 + gpx8E1	pVD54	gpx8E2 + gpx8E4	pcDNA3.1$^+$	NeoRH2 + gpx7E3
pES103	pES102	NeoRH1 + gpx8fE5	pES102	NeoRH2 + gpxfE6		
pES104	pES101	NeoRH1 + gpx7E6	pES101	NeoRH2 + gpx7E5		
pES105	pES103	NeoRH1 + gpx8E10	pES103	NeoRH2 + gpx8E9		

by MonoQ anion exchange column (GE Healthcare) and Superdex 200 size-exclusion column (GE Healthcare).

Antibodies, reagent, and immunological techniques

Rabbit antibodies to ERp57 (GTX100297), and to ERp72 (GTX115263) were purchased from GeneTex. For the detection of proteins fused with a triple FLAG tag, mouse anti-FLAG M2 antibody conjugated with horseradish peroxidase (Sigma A8592) was used. Rabbit antibody to PDI has been published (50). Antibodies to ERp46 and P5 were used as described previously (10). Immunoloblotting was performed using standard methods. The protein bands were visualized using an appropriate secondary antibody, Clarity Western ECL substrate (Bio-Rad) and ChemiDoc touch imaging system (Bio-Rad). The images were processed with Image laboratory software (Bio-Rad).

Analysis of the redox states of GPx7, GPx8, PDI, and their mutants

Purified GPx7, the luminal domain of GPx8, PDIs, and their mutants were separately reduced with 10 mM DTT for 10 min at 30 °C followed by DTT removal through a PD-10 column (GE Healthcare) pre-equilibrated with 50 mM Tris/HCl (pH 7.4) buffer containing 300 mM NaCl. To analyze the redox status of GPx7, GPx8, and their mutants, different concentrations (10, 50, and 200 μM) of H_2O_2 were mixed with 1 μM reduced GPx7, GPx8, or their mutants in degassed buffer containing 50 mM Tris/HCl (pH 7.4) and 300 mM NaCl at 30 °C. For PDI oxidation assays, 10 μM reduced PDI was incubated with 1 μM GPx7, GPx8, or their mutants, and reactions were initiated by adding 10, 50, or 200 μM of H_2O_2. At the indicated time points, the samples were quenched using 1 mM mal-PEG 2000 (NOF Corporation). The reaction mixture was boiled for 3 min after addition of an equal volume of 2× Laemmli buffer. All of the samples were run through nonreducing SDS-PAGE followed by staining with Coomassie Brilliant Blue (CBB) (Nacalai Tesque). The gel images were captured by using ChemiDoc touch imaging system (Bio-Rad).

Oxidative folding assay of RNase A

RNase A from bovine pancreas (Sigma–Aldrich) was reduced and denatured with 100 mM DTT and 6 K guanidinium hydrochloride. The sample was passed through a PD-10 column (GE Healthcare) pre-equilibrated with 10 mM HCl aq. to remove the reducing and denaturing reagents. Reduced/denatured RNase A was diluted to 20 μM (~50-fold dilution) and incubated with 1 μM GPx7 or its mutant and 10 μM PDI in a buffer (50 mM Tris/HCl, pH 7.4, and 300 mM NaCl) at 30 °C, and the reactions were initiated by adding 50 μM of H_2O_2. At the indicated time points, the samples were quenched using 1 mM 4-acetamide-4′-maleimidylstilbene-2,2′-disulfonic acid (AMS; Molecular Probes, Inc.). All samples were separated by nonreducing SDS-PAGE followed by staining with CBB. The gel images were captured by the ChemiDoc touch imaging system (Bio-Rad). The recovery of RNase A activity was measured by monitoring the linear increase in absorbance at 295 nm on a U-3900 spectrophotometer (Hitachi) at 30 °C after addition of 1.25 mM cytidine 2′,3′-cyclic monophosphate monosodium salt (Sigma–Aldrich) to reaction mixtures at the indicated time points.

NADPH consumption assay

NADPH consumption coupled with GPx7-catalyzed PDI oxidation was monitored by measuring absorbance change at 340

nm using a SH-9000 microplate reader (Corona Electric Co.). The solution was first prepared by mixing 1 μM GPx7 WT or GPx7 C86A, 5–50 μM reduced PDI, 1 mM GSH, 1 unit GSH reductase (GR), and 200 μM NADPH in a buffer (50 mM Tris/HCl, pH 7.4, and 300 mM NaCl), and the reactions were initiated at 30 °C by adding 50 μM of H_2O_2 to the solution. The initial NADPH consumption rates were calculated by considering the decrease of absorbance at 340 nm during the initial reaction time of 30 s with a molar extinction coefficient value of 6200 M^{-1} cm^{-1} for NADPH.

Preferential PDI oxidation by GPx7 in vitro

5 μM each of purified PDI family members (PDI, P5, ERp46, ERp57, and ERp72) was mixed with 0.5 μM GPx7. The reactions were initiated by adding 50 μM of H_2O_2 to the solutions. At the indicated time points, the samples were subjected to 2 mM mal-PEG 2000 (NOF Corporation) followed by immunoblotting with the corresponding anti-PDI antibodies.

Cell culture, transfection, and sample preparation

The cells were transfected with plasmids using Effectene (Qiagen). For the transfection, HeLa cells were plated in 10-cm dishes at 8×10^5 cells/well, cultured for 24 h, and transfected with an appropriate plasmid, following the manufacturer's instruction. The amount of plasmid DNA used for the transfection was 2 μg for pcDNA3.1$^+$ and pCMV-Gg PRX4 (encoding PRX4-FLAG) (10), 6 μg for pES104 (encoding GPx7-FLAG), and 6 μg for pES105 (encoding full-length GPx8-FLAG). The larger amount of plasmid DNA was used for transfection with the latter two plasmids because the levels of protein production from these plasmids were smaller than that from the former one when the same amount of plasmid DNA was used. At 24 h after the transfection, the cells were treated with or without 0.5 mM H_2O_2 for 10 min, washed twice with PBS, treated with 10% TCA, and subjected to alkylation with NEM essentially as described (51).

Immunoprecipitation

500 μg of NEM-treated cell lysate prepared as described above was diluted with ice-cold KI buffer (2% (w/v) Triton X-100, 50 mM Tris-HCl, pH 8.0, 150 mM NaCl, 1 mM EDTA) and centrifuged at 15,000 × *g* for 10 min at 4 °C to obtain NEM-treated cleared cell lysate. To purify FLAG-tagged proteins (PRX4-FLAG, GPx7-FLAG, or GPx8-FLAG) from the cleared cell lysate, 50 μl of prewashed anti-FLAG M2 magnetic beads (Sigma) were incubated with the NEM-treated cleared cell lysate at 4 °C for 3 h. The immune complexes were collected by magnetization and washed four times with 800 μl of ice-cold high-salt buffer (1% (w/v) Triton X-100, 50 mM Tris-HCl, pH 8.0, 1 M NaCl, 1 mM EDTA) and once with 800 μl of 10 mM Tris-HCl (pH 8.0). The immunoisolates were then released by incubating the sample at 37 °C for 1 h with 65 μl of 2× Laemmli sample buffer supplemented with 10 mM NEM, 2 μg/ml pepstatin A, 1 mM benzamidine, and 1 mM phenylmethylsulfonyl fluoride.

Data availability

All data described are contained within the article.

Acknowledgments—We are grateful to Dr. Lloyd Ruddock (University of Oulu) for providing plasmids for overexpression of GPx7 and GPx8 in *E. coli*.

Author contributions—S. K. and K. I. conceptualization; S. K. and K. I. resources; S. K., E. F. S., N. H., M. O., and H. K. data curation; S. K., E. F. S., N. H., and M. O. formal analysis; S. K., M. O., and K. I. supervision; S. K., E. F. S., and K. I. funding acquisition; S. K., E. F. S., and H. K. validation; S. K., E. F. S., N. H., M. O., H. K., and K. I. investigation; S. K. and K. I. project administration; S. K. and K. I. writing-review and editing; E. F. S., N. H., and H. K. writing-original draft.

Funding and additional information—This work was supported by Japan Society for the Promotion of Science KAKENHI Grants JP17H06521 (to S. K.), JP19K16092 (to S. K.), and JP19H02881 (to H. K.) and Grants-in-Aid for Scientific Research for Scientific Research 26116005 and 18H03978 from the Ministry of Education, Culture, Sports, Science and Technology (to K. I.).

Conflict of interest—The authors declare that they have no conflicts of interest with the contents of this article.

Abbreviations—The abbreviations used are: ER, endoplasmic reticulum; PDI, protein-disulfide isomerase; GPx7/8, glutathione peroxidase-7/8; Prx4, peroxiredoxin-4; C_P, peroxidatic cysteine residue; C_R, resolving cysteine residue; mal-PEG 2k, maleimidyl PEG-2000; NEM, *N*-maleimide; CBB, Coomassie Brilliant Blue; AMS, 4-acetamide-4′-maleimidylstilbene-2,2′-disulfonic acid; GR, glutathione reductase.

References

1. Hatahet, F., and Ruddock, L. W. (2009) Protein disulfide isomerase: a critical evaluation of its function in disulfide bond formation. *Antioxid. Redox Signal.* **11,** 2807–2850 CrossRef Medline
2. Bulleid, N. J., and Ellgaard, L. (2011) Multiple ways to make disulfides. *Trends Biochem. Sci.* **36,** 485–492 CrossRef Medline
3. Sato, Y., and Inaba, K. (2012) Disulfide bond formation network in the three biological kingdoms, bacteria, fungi and mammals. *FEBS J.* **279,** 2262–2271 CrossRef Medline
4. Okumura, M., Kadokura, H., and Inaba, K. (2015) Structures and functions of protein disulfide isomerase family members involved in proteostasis in the endoplasmic reticulum. *Free Radic. Biol. Med.* **83,** 314–322 CrossRef Medline
5. Matsusaki, M., Kanemura, S., Kinoshita, M., Lee, Y. H., Inaba, K., and Okumura, M. (2020) The protein disulfide isomerase family: from proteostasis to pathogenesis. *Biochim. Biophys. Acta* **1864,** 129338 CrossRef
6. Araki, K., and Inaba, K. (2012) Structure, mechanism, and evolution of Ero1 family enzymes. *Antioxid. Redox Signal.* **16,** 790–799 CrossRef Medline
7. Appenzeller-Herzog, C., and Ellgaard, L. (2008) The human PDI family: versatility packed into a single fold. *Biochim. Biophys. Acta* **1783,** 535–548 CrossRef Medline
8. Kanemura, S., Okumura, M., Yutani, K., Ramming, T., Hikima, T., Appenzeller-Herzog, C., Akiyama, S., and Inaba, K. (2016) Human ER oxidoreductin-1α (Ero1α) undergoes dual regulation through complementary redox

interactions with protein-disulfide isomerase. *J. Biol. Chem.* **291,** 23952–23964 CrossRef Medline
9. Ramming, T., Okumura, M., Kanemura, S., Baday, S., Birk, J., Moes, S., Spiess, M., Jenö, P., Bernèche, S., Inaba, K., and Appenzeller-Herzog, C. (2015) A PDI-catalyzed thiol-disulfide switch regulates the production of hydrogen peroxide by human Ero1. *Free Radic. Biol. Med.* **83,** 361–372 CrossRef Medline
10. Sato, Y., Kojima, R., Okumura, M., Hagiwara, M., Masui, S., Maegawa, K., Saiki, M., Horibe, T., Suzuki, M., and Inaba, K. (2013) Synergistic cooperation of PDI family members in peroxiredoxin 4–driven oxidative protein folding. *Sci. Rep.* **3,** 2456 CrossRef Medline
11. Zito, E., Melo, E. P., Yang, Y., Wahlander, A., Neubert, T. A., and Ron, D. (2010) Oxidative protein folding by an endoplasmic reticulum-localized peroxiredoxin. *Mol. Cell* **40,** 787–797 CrossRef Medline
12. Tavender, T. J., Springate, J. J., and Bulleid, N. J. (2010) Recycling of peroxiredoxin IV provides a novel pathway for disulphide formation in the endoplasmic reticulum. *EMBO J.* **29,** 4185–4197 CrossRef Medline
13. Oka, O. B., Pringle, M. A., Schopp, I. M., Braakman, I., and Bulleid, N. J. (2013) ERdj5 is the ER reductase that catalyzes the removal of non-native disulfides and correct folding of the LDL receptor. *Mol. Cell* **50,** 793–804 CrossRef Medline
14. Ushioda, R., Hoseki, J., Araki, K., Jansen, G., Thomas, D. Y., and Nagata, K. (2008) ERdj5 is required as a disulfide reductase for degradation of misfolded proteins in the ER. *Science* **321,** 569–572 CrossRef Medline
15. Maegawa, K. I., Watanabe, S., Noi, K., Okumura, M., Amagai, Y., Inoue, M., Ushioda, R., Nagata, K., Ogura, T., and Inaba, K. (2017) The highly dynamic nature of ERdj5 is key to efficient elimination of aberrant protein oligomers through ER-associated degradation. *Structure* **25,** 846–857.e4 CrossRef Medline
16. Hagiwara, M., Maegawa, K., Suzuki, M., Ushioda, R., Araki, K., Matsumoto, Y., Hoseki, J., Nagata, K., and Inaba, K. (2011) Structural basis of an ERAD pathway mediated by the ER-resident protein disulfide reductase ERdj5. *Mol. Cell* **41,** 432–444 CrossRef Medline
17. Ellgaard, L., and Helenius, A. (2003) Quality control in the endoplasmic reticulum. *Nat. Rev. Mol. Cell Biol.* **4,** 181–191 CrossRef Medline
18. Byun, H., Gou, Y., Zook, A., Lozano, M. M., and Dudley, J. P. (2014) ERAD and how viruses exploit it. *Front. Microbiol.* **5,** 330 CrossRef Medline
19. Tsai, B., Rodighiero, C., Lencer, W. I., and Rapoport, T. A. (2001) Protein disulfide isomerase acts as a redox-dependent chaperone to unfold cholera toxin. *Cell* **104,** 937–948 CrossRef Medline
20. Tavender, T. J., and Bulleid, N. J. (2010) Molecular mechanisms regulating oxidative activity of the Ero1 family in the endoplasmic reticulum. *Antioxid. Redox Signal.* **13,** 1177–1187 CrossRef Medline
21. Masui, S., Vavassori, S., Fagioli, C., Sitia, R., and Inaba, K. (2011) Molecular bases of cyclic and specific disulfide interchange between human ERO1α protein and protein-disulfide isomerase (PDI). *J. Biol. Chem.* **286,** 16261–16271 CrossRef Medline
22. Inaba, K., Masui, S., Iida, H., Vavassori, S., Sitia, R., and Suzuki, M. (2010) Crystal structures of human Ero1α reveal the mechanisms of regulated and targeted oxidation of PDI. *EMBO J.* **29,** 3330–3343 CrossRef Medline
23. Ramming, T., Kanemura, S., Okumura, M., Inaba, K., and Appenzeller-Herzog, C. (2016) Cysteines 208 and 241 in Ero1α are required for maximal catalytic turnover. *Redox Biol.* **7,** 14–20 CrossRef Medline
24. Tavender, T. J., and Bulleid, N. J. (2010) Peroxiredoxin IV protects cells from oxidative stress by removing H_2O_2 produced during disulphide formation. *J. Cell Sci.* **123,** 2672–2679 CrossRef Medline
25. Zhu, L., Yang, K., Wang, X., Wang, X., and Wang, C. C. (2014) A novel reaction of peroxiredoxin 4 towards substrates in oxidative protein folding. *PLoS One* **9,** e105529 CrossRef Medline
26. Benham, A. M., van Lith, M., Sitia, R., and Braakman, I. (2013) Ero1–PDI interactions, the response to redox flux and the implications for disulfide bond formation in the mammalian endoplasmic reticulum. *Philos. Trans. R. Soc. Lond. B Biol. Sci.* **368,** 20110403 CrossRef Medline
27. Wajih, N., Hutson, S. M., and Wallin, R. (2007) Disulfide-dependent protein folding is linked to operation of the vitamin K cycle in the endoplasmic reticulum: a protein disulfide isomerase–VKORC1 redox enzyme complex appears to be responsible for vitamin K_1 2,3-epoxide reduction. *J. Biol. Chem.* **282,** 2626–2635 CrossRef Medline
28. Cao, Z., van Lith, M., Mitchell, L. J., Pringle, M. A., Inaba, K., and Bulleid, N. J. (2016) The membrane topology of vitamin K epoxide reductase is conserved between human isoforms and the bacterial enzyme. *Biochem. J.* **473,** 851–858 CrossRef Medline
29. Nguyen, V. D., Saaranen, M. J., Karala, A. R., Lappi, A. K., Wang, L., Raykhel, I. B., Alanen, H. I., Salo, K. E., Wang, C. C., and Ruddock, L. W. (2011) Two endoplasmic reticulum PDI peroxidases increase the efficiency of the use of peroxide during disulfide bond formation. *J. Mol. Biol.* **406,** 503–515 CrossRef Medline
30. Wang, L., Zhang, L., Niu, Y., Sitia, R., and Wang, C. C. (2014) Glutathione peroxidase 7 utilizes hydrogen peroxide generated by Ero1α to promote oxidative protein folding. *Antioxid. Redox Signal.* **20,** 545–556 CrossRef Medline
31. Bosello-Travain, V., Conrad, M., Cozza, G., Negro, A., Quartesan, S., Rossetto, M., Roveri, A., Toppo, S., Ursini, F., Zaccarin, M., and Maiorino, M. (2013) Protein disulfide isomerase and glutathione are alternative substrates in the one Cys catalytic cycle of glutathione peroxidase 7. *Biochim. Biophys. Acta* **1830,** 3846–3857 CrossRef Medline
32. Brigelius-Flohé, R., and Maiorino, M. (2013) Glutathione peroxidases. *Biochim. Biophys. Acta* **1830,** 3289–3303 CrossRef Medline
33. Maiorino, M., Bosello-Travain, V., Cozza, G., Miotto, G., Roveri, A., Toppo, S., Zaccarin, M., and Ursini, F. (2015) Understanding mammalian glutathione peroxidase 7 in the light of its homologs. *Free Radic. Biol. Med.* **83,** 352–360 CrossRef Medline
34. Chen, Y. I., Wei, P. C., Hsu, J. L., Su, F. Y., and Lee, W. H. (2016) NPGPx (GPx7): a novel oxidative stress sensor/transmitter with multiple roles in redox homeostasis. *Am. J. Transl. Res.* **8,** 1626–1640 Medline
35. Wei, P. C., Hsieh, Y. H., Su, M. I., Jiang, X., Hsu, P. H., Lo, W. T., Weng, J. Y., Jeng, Y. M., Wang, J. M., Chen, P. L., Chang, Y. C., Lee, K. F., Tsai, M. D., Shew, J. Y., and Lee, W. H. (2012) Loss of the oxidative stress sensor NPGPx compromises GRP78 chaperone activity and induces systemic disease. *Mol. Cell* **48,** 747–759 CrossRef Medline
36. Utomo, A., Jiang, X., Furuta, S., Yun, J., Levin, D. S., Wang, Y. C., Desai, K. V., Green, J. E., Chen, P. L., and Lee, W. H. (2004) Identification of a novel putative non-selenocysteine containing phospholipid hydroperoxide glutathione peroxidase (NPGPx) essential for alleviating oxidative stress generated from polyunsaturated fatty acids in breast cancer cells. *J. Biol. Chem.* **279,** 43522–43529 CrossRef Medline
37. Peng, D., Belkhiri, A., Hu, T., Chaturvedi, R., Asim, M., Wilson, K. T., Zaika, A., and El-Rifai, W. (2012) Glutathione peroxidase 7 protects against oxidative DNA damage in oesophageal cells. *Gut* **61,** 1250–1260 CrossRef Medline
38. Chang, Y. C., Yu, Y. H., Shew, J. Y., Lee, W. J., Hwang, J. J., Chen, Y. H., Chen, Y. R., Wei, P. C., Chuang, L. M., and Lee, W. H. (2013) Deficiency of NPGPx, an oxidative stress sensor, leads to obesity in mice and human. *EMBO Mol. Med.* **5,** 1165–1179 CrossRef Medline
39. Ramming, T., Hansen, H. G., Nagata, K., Ellgaard, L., and Appenzeller-Herzog, C. (2014) GPx8 peroxidase prevents leakage of H_2O_2 from the endoplasmic reticulum. *Free Radic. Biol. Med.* **70,** 106–116 CrossRef Medline
40. Tosatto, S. C., Bosello, V., Fogolari, F., Mauri, P., Roveri, A., Toppo, S., Flohé, L., Ursini, F., and Maiorino, M. (2008) The catalytic site of glutathione peroxidases. *Antioxid. Redox Signal.* **10,** 1515–1526 CrossRef Medline
41. Toppo, S., Vanin, S., Bosello, V., and Tosatto, S. C. (2008) Evolutionary and structural insights into the multifaceted glutathione peroxidase (Gpx) superfamily. *Antioxid. Redox Signal.* **10,** 1501–1514 CrossRef Medline
42. Antosiewicz, J., McCammon, J. A., and Gilson, M. K. (1994) Prediction of pH-dependent properties of proteins. *J. Mol. Biol.* **238,** 415–436 CrossRef Medline
43. Winterbourn, C. C., and Hampton, M. B. (2008) Thiol chemistry and specificity in redox signaling. *Free Radic. Biol. Med.* **45,** 549–561 CrossRef Medline
44. Kojima, R., Okumura, M., Masui, S., Kanemura, S., Inoue, M., Saiki, M., Yamaguchi, H., Hikima, T., Suzuki, M., Akiyama, S., and Inaba, K. (2014) Radically different thioredoxin domain arrangement of ERp46, an efficient disulfide bond introducer of the mammalian PDI family. *Structure* **22,** 431–443 CrossRef Medline
45. Wang, L., Li, S. J., Sidhu, A., Zhu, L., Liang, Y., Freedman, R. B., and Wang, C. C. (2009) Reconstitution of human Ero1-Lα/protein-disulfide

isomerase oxidative folding pathway *in vitro*: position-dependent differences in role between the a and a' domains of protein-disulfide isomerase. *J. Biol. Chem.* **284,** 199–206 CrossRef Medline

46. Nelson, J. W., and Creighton, T. E. (1994) Reactivity and ionization of the active site cysteine residues of DsbA, a protein required for disulfide bond formation *in vivo*. *Biochemistry* **33,** 5974–5983 CrossRef Medline
47. Gutscher, M., Sobotta, M. C., Wabnitz, G. H., Ballikaya, S., Meyer, A. J., Samstag, Y., and Dick, T. P. (2009) Proximity-based protein thiol oxidation by H_2O_2-scavenging peroxidases. *J. Biol. Chem.* **284,** 31532–31540 CrossRef Medline
48. Jessop, C. E., Watkins, R. H., Simmons, J. J., Tasab, M., and Bulleid, N. J. (2009) Protein disulphide isomerase family members show distinct substrate specificity: P5 is targeted to BiP client proteins. *J. Cell Sci.* **122,** 4287–4295 CrossRef Medline
49. Meunier, L., Usherwood, Y. K., Chung, K. T., and Hendershot, L. M. (2002) A subset of chaperones and folding enzymes form multiprotein complexes in endoplasmic reticulum to bind nascent proteins. *Mol. Biol. Cell* **13,** 4456–4469 CrossRef Medline
50. Okumura, M., Kadokura, H., Hashimoto, S., Yutani, K., Kanemura, S., Hikima, T., Hidaka, Y., Ito, L., Shiba, K., Masui, S., Imai, D., Imaoka, S., Yamaguchi, H., and Inaba, K. (2014) Inhibition of the functional interplay between endoplasmic reticulum (ER) oxidoreductin-1α (Ero1α) and protein-disulfide isomerase (PDI) by the endocrine disruptor bisphenol A. *J. Biol. Chem.* **289,** 27004–27018 CrossRef Medline
51. Fujimoto, T., Nakamura, O., Saito, M., Tsuru, A., Matsumoto, M., Kohno, K., Inaba, K., and Kadokura, H. (2018) Identification of the physiological substrates of PDIp, a pancreas-specific protein-disulfide isomerase family member. *J. Biol. Chem.* **293,** 18421–18433 CrossRef Medline